Structural Engineering and Mechanics, *Vol. 68, No. 5 (2018) 575-589*
DOI: https://doi.org/10.12989/sem.2018.68.5.575

A new method to predict the critical incidence angle for buildings under near-fault motions

Paolo E. Sebastiani[a], Laura Liberatore*, Andrea Lucchini[b] and Fabrizio Mollaioli[c]

Department of Structural and Geotechnical Engineering, Sapienza University of Rome, Via Gramsci 53, 00197 Rome, Italy

(Received April 12, 2018, Revised October 12, 2018, Accepted October 23, 2018)

Abstract. It is well known that the incidence angle of seismic excitation has an influence on the structural response of buildings, and this effect can be more significant in the case of near-fault signals. However, current seismic codes do not include detailed requirements regarding the direction of application of the seismic action and they have only recently introduced specific provisions about near-fault earthquakes. Thus, engineers have the task of evaluating all the relevant directions or the most critical conditions case by case, in order to avoid underestimating structural demand. To facilitate the identification of the most critical incidence angle, this paper presents a procedure which makes use of a two-degree of freedom model for representing a building. The proposed procedure makes it possible to avoid the extensive computational effort of multiple dynamic analyses with varying angles of incidence of ground motion excitation, which is required if a spatial multi-degree of freedom model is used for representing a building. The procedure is validated through the analysis of two case studies consisting of an eight- and a six-storey reinforced concrete frame building, selected as representative of existing structures located in Italy. A set of 124 near-fault ground motion records oriented along 8 incidence angles, varying from 0 to 180 degrees, with increments of 22.5 degrees, is used to excite the structures. Comparisons between the results obtained with detailed models of the two structures and the proposed procedure are used to show the accuracy of the latter in the prediction of the most critical angle of seismic incidence.

Keywords: near-fault; directionality; incidence angle; dynamic analysis; spatial building model

1. Introduction

It is common knowledge that near-fault pulse-like ground motions may cause large displacement and strength demands in structures, and increase their risk of earthquake-induced collapse (Haselton *et al.* 2011, Liel *et al.* 2011, Decanini *et al.* 2012). In the proximity of an active fault system, ground motions are significantly affected by the faulting mechanism, the possible static deformation of the ground surface associated with fling-step effects, as well as the direction of rupture propagation relative to the site (e.g. forward directivity) (Somerville *et al.* 1997, Mavroeidis and Papageorgiou 2003, Kalkan and Kunnath 2006, Mollaioli *et al.* 2006, Baker 2007). As shown by several past earthquakes, the latter may produce extensive damage in structures. One of the most representative examples of building failure due to near-fault directivity is that of the Olive View Hospital in California, which collapsed after the 1971 San Fernando earthquake (Chopra and Chintanapakdee 2001).

Over the last few years, a number of works have focused on the effects of near-fault motions on different types of structures (e.g., Tabatabaei and Saffari 2011, Mazza *et al.* 2017) and on the definition of proper ground motion parameters and methods to be used for design and assessment purposes (e.g., Moustafa and Takewaki 2010, Cao and Ronagh 2014). However, few studies have addressed the issue of the effects of the incidence angle on structures subjected to near-fault pulse-like excitations.

Concerning current seismic codes, they generally require that at least the two horizontal ground motion components should be applied in three-dimensional response history analysis of structures. For instance, both the ASCE/SEI 7-10 (2010) and the California Building Code (ICBO 2010) require that in the case of near-fault motions, the components shall be first rotated to the fault-normal and the fault-parallel (FN/FP) directions and then applied to the principal directions of the structure. This requirement derives from the assumption that the incidence angle corresponding to the FN/FP directions is the most critical for structural response. Approximations produced by this assumption are examined in Kalkan and Kwong (2014) and in Athanatopoulou (2005).

FEMA356 (2000) prescribes that seismic motion be applied along the "structural axes", but no definition of the latter is given. In particular, it is not clear if these axes coincide with the principal axes of the structure, and, in this case, how they are determined in complex structures with asymmetric plans. Besides, it is important to note that the application of ground motion components along the principal structural axes may not be the right choice. Hosseini and Salemi (2008) have demonstrated, indeed, that the peak deformation demand can be underestimated when

*Corresponding author, Assistant Professor
E-mail: laura.liberatore@uniroma1.it
[a]Researcher
[b]Assistant Professor
[c]Associate Professor

ISSN: 1225-4568 (Print), 1598-6217 (Online)

the components are applied along the principal axes of an inelastic structure.

According to Eurocode 8 (2004), horizontal seismic motion shall be applied along any relevant directions and similarly, in the ASCE/SEI 7-10 (2010), the directions of application of the design seismic forces shall be those which will produce the most critical effects. Therefore, the designer should evaluate all the critical directions for the structure, in order to avoid underestimating seismic demand. This evaluation is necessary not only for complex and irregular structures, but also for regular structures. In fact, even for single storey symmetric buildings without mass eccentricity, the incident angle was found to significantly influence the response (Tsourekas *et al.* 2009). Also, Fontara *et al.* (2012) showed that the maximum value of the overall structural damage index does not occur when the seismic motion acts along the structural axes. In the case studies analysed in Cantagallo *et al.* (2012, 2015), the ground motion records that generate the highest demands are applied along the most flexible structural direction, because of the high energy content of the records in this direction.

Reyes and Kalkan (2015) used 3D models of single-storey structures, characterized by both symmetric and asymmetric layouts, to evaluate the possible occurrence of conservative estimates of selected engineering demand parameters when near-fault ground motion is rotated in the FN/FP direction. Based on the demands obtained from an ensemble of exciting ground motions, they concluded that the critical angle, corresponding to the largest response over all rotation angles, varies in general with the ground motion and the considered engineering demand parameter. Therefore, it seems very difficult to define a-priori a specific orientation for the seismic action that maximizes demands without performing time history analyses on the building.

Rigato and Medina (2007) examined the influence of directionality on drift and ductility demands of symmetric and asymmetric reinforced concrete structures. They found that the ratio between the maximum inelastic deformation obtained for a given angle of incidence and that obtained for an incidence angle corresponding to the principal building axes tends to increase with the fundamental period and varies, on average, between 1.1 and 1.6 for both torsionally balanced and torsionally unbalanced systems. In general, the critical angle is structure specific and depends on the level of the inelastic demand. It is, therefore, difficult to determine a-priori. This explains why, currently, the most commonly adopted approach for the analysis of spatial models is the application of bi-directional ground motion at various angles with respect to the structure principal directions. The variation of the response with respect to the incidence angle is estimated and the most critical angle is identified, but a large computational effort is usually required.

In order to avoid a multiple analysis of the structure that involves varying the angle of seismic incidence, Emami and Halabian (2005) investigated the effect of the orientation of ground motion directionality on different engineering demand parameters, and proposed ranges of amplification factors for the values obtained when the ground motion is oriented along non-principal directions instead of the principal ones.

Motivated by the same goal, this work presents a computationally efficient procedure to predict the most critical incidence angle that employs a simplified model for the structure. The procedure is applied to two reinforced concrete structures subjected to a set of 124 near-fault ground motion records oriented along 8 incidence angles, which vary from 0 to 180 degrees, with an increment of 22.5 degrees. The two analysed structures, eight- and six-storey tall, were selected as representative of existing buildings located in Italy. Comparisons with results of non-linear dynamic analyses using 3D models for the structures are performed to verify the predictive accuracy of the proposed procedure.

2. Aim of the work and procedure outline

The purpose of this research is to propose a procedure to predict the most critical angle of application of the seismic load for a given structure. This section presents the outline of the procedure, which will be applied and validated in the next sections.

The procedure can be summarized as follows (see also Fig. 1):

- Create a 3D non-linear model of the structure.
- Determine the capacity curves along the principal axes of the structure through Non-linear Static Pushover Analyses (NLSPA).
- Calibrate a 2DOF non-linear equivalent model using the results of the previous analyses.
- Select a Ground Motion (GM), which defines the seismic load at the site.
- Analyse the response of the 2DOF model, subjected to the selected GM, varying the incidence angle.
- Identify the most critical angle of incidence ϑ_{cr}, which causes the maximum displacement U of the 2DOF.
- Analyse the 3D model subjected to the selected GM applied according to the angle ϑ_{cr} by using a Non-linear Time-History Analysis (NLTHA).
- Repeat the procedure, if necessary, for other GMs of interest.

3. Case studies

3.1 Ground motion database

The ground motion database, used as input for the non-linear dynamic analyses, consists of 124 pairs of horizontal records from 27 earthquakes (see Appendix). The moment magnitude of these earthquakes ranges from 5.0 (2000 Yountville earthquake) to 7.6 (1999 Chi-Chi, Taiwan earthquake). Soil conditions are mainly characterized by type C and D, as defined in the NEHRP 2004 site classification based on the preferred V_{s30} values. The closest distance from the fault projection, ClstD, varies from 0.1 km to 102.4 km. The selection of the records was based on

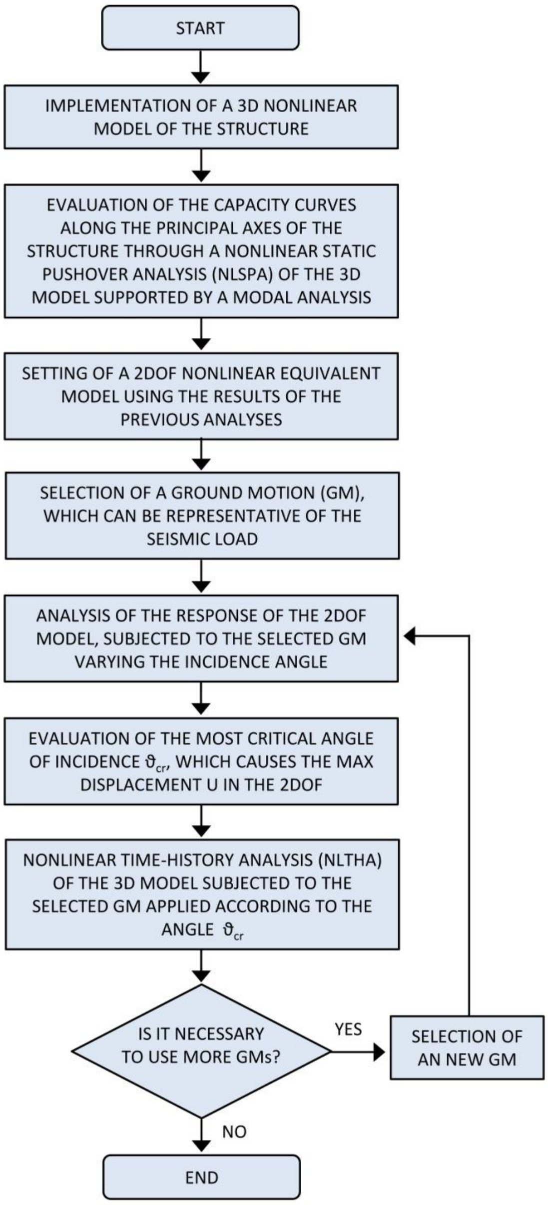

Fig. 1 Flow chart of the procedure

the presence of pulses due do forward-directivity rather than on distance from the fault (see also Mollaioli *et al.* 2014). Specifically, the selected ground motions satisfy the geometric conditions for forward directivity defined in Somerville *et al.* (1997), show polarization in the fault-normal direction in their velocity time histories and have a clear pulse in the fault-normal direction. Some records of the database are not characterized by short fault-to-site distances. However, 90% of them have distances less than 20 km and only four records have distances greater than 30 km.

Each pair of horizontal recordings was decomposed to the fault-normal (FN) and fault-parallel (FP) components using known planer transformation equations. In the dynamic analyses, the 124 pairs of FN and FP components are applied to the building in a set of 8 different directions, similarly to what was done in Mollaioli *et al.* (2014), as

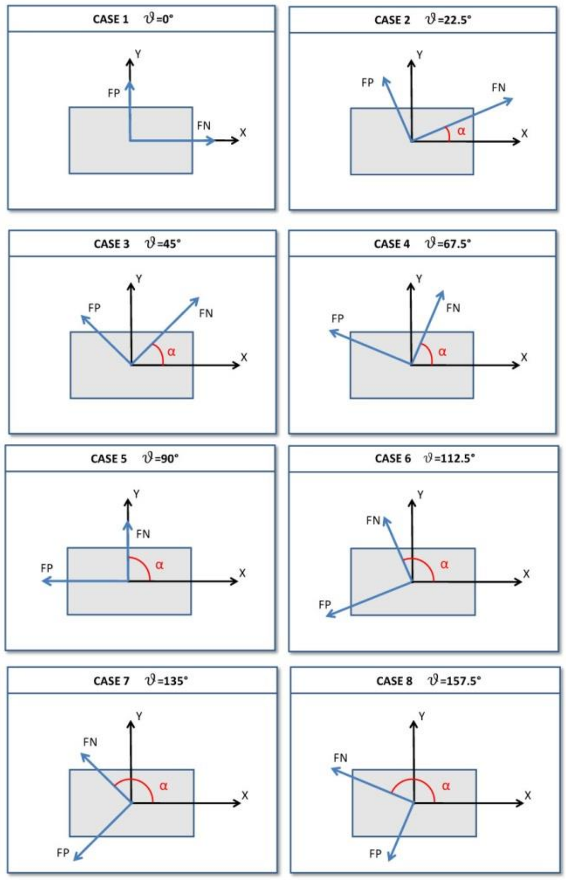

Fig. 2 Considered set of incidence angles

shown in Fig. 2. Therefore, if X and Y are the principal axes of the building, the FN and FP components are rotated $\vartheta°$ away from the X axis. The angle $\vartheta°$ varies from 0° to 180° with increments of 22.5°. Note that the angles 0° and 180° represent the same direction, only the orientation changes.

3.2 Buildings

The two reinforced concrete eight-storey and six-storey buildings were designed according to the former Italian code DM96 (1996), and were selected as representative of existing buildings located in a medium seismic zone, i.e., “zone 2” according to the seismic hazard classification of DM96. Fig. 3 shows two lateral views of the eight-storey building. The structure is a rectangular multi-bay structure 28×18 m^2 in plan and 28 m tall.

Fig. 4 gives the dimensions and reinforcement of both beams and columns of the eight-storey building. At the base of the building, the cross sections of the columns (denoted with the letters A, B and E in Fig. 4) are 90×45 cm^2, 50×50 cm^2 and 50×35 cm^2. From the 5th level to the top of the building the column sections B and E are reduced to 40×40 cm^2 and 45×30 cm^2 (sections D and C, respectively). The cross sections of the interior beams are 80×24 cm^2 and 100×24 cm^2, while those of the beams along the perimeter are 30×60 cm^2 (sections from F to H in Fig. 4).

The six-storey building is also a rectangular multi-bay structure 21 m tall having the same dimensions in plan as

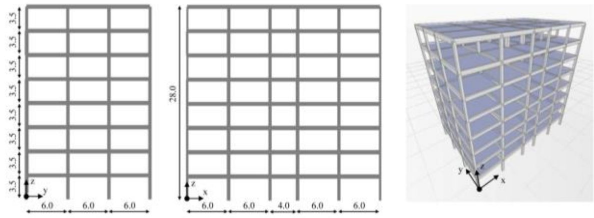

Fig. 3 Lateral and perspective views of the 8-storey frame model (dimensions in m)

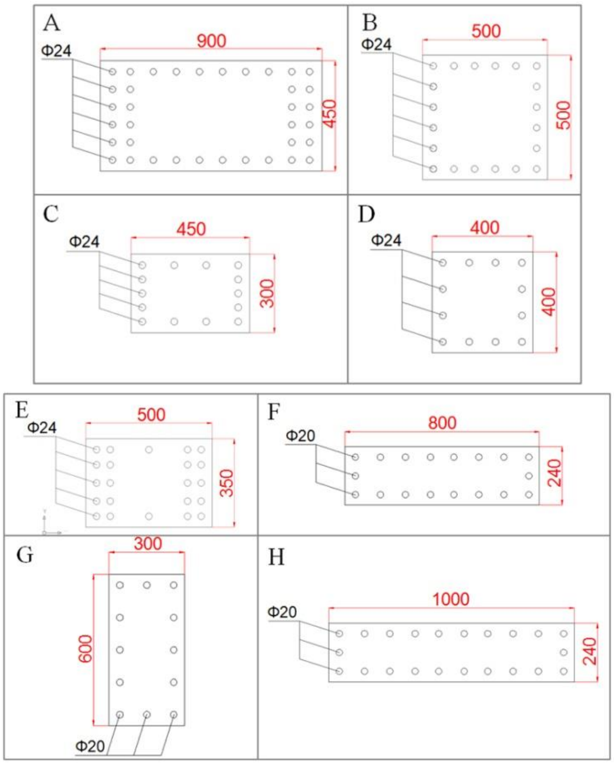

Fig. 4 Structural members of the 8-storey building: Cross-sections and longitudinal reinforcement (dimensions in mm). A-B-E and D: Columns at floors 1-4, and 5-8, respectively. F and H: Interior beams (all floors), G perimeter beams (all floors)

the eight-storey building (see Fig. 5). The dimensions of the cross sections of the columns and the beams are the same for the two buildings with only small differences in the reinforcement.

The gravity loads that are applied to the structures are: structural, non-structural and live loads. The first two include the self-weight of the structural members, exterior walls, partitions and coatings-coverings. The live load is that of a residential building. The values of all loads used in the design of the eight-storey and the six-storey buildings are given in Tables 1-2, respectively.

The response of the selected buildings is estimated via non-linear dynamic analyses run in OpenSees (McKenna 1997). Beams and columns of the structures are modelled using distributed plasticity, flexibility-based nonlinear beam-column elements with fibre-sections. The masses are concentrated at the nodes and the floor stiffness is modelled with rigid diaphragm constraints. Damping ratio, assumed proportional to mass and tangent stiffness, is equal to 5%. Geometric non-linearities are included using P-Delta transformations. The properties of the materials are given in Table 3 and Fig. 6.

The periods of the first three modes of vibration of the frame models, obtained after the application of gravity loads, are given for both the eight-storey and the six-storey building in Table 4. Fig. 7 shows the shape of the first three modes of vibration of the eight-storey building. The six-storey building is characterized by similar modal shapes, i.e., two translational modes along the in-plan directions Y and X (mode 1 and 2, respectively), and a torsional mode (mode 3). In the Y direction, the mass participation ratio of mode 1 is equal to 0.73 and 0.78, for the eight- and six-storey building, respectively. In the X direction, where the

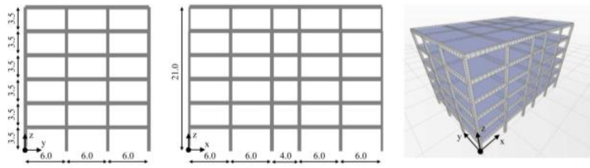

Fig. 5 Lateral and perspective views of the six-storey frame model (dimensions in m)

Table 1 Design loads for the eight-storey building

Type of load	Value	Unit
Structural permanent loads		
Slab self-weight	3.75	kN/m^2
Non-structural permanent loads		
Floor finish	0.80	kN/m^2
Screed	1.80	kN/m^2
Plaster finish	0.30	kN/m^2
Ceiling system	1.50	kN/m^2
Partitions (roof excluded)	1.20	kN/m^2
Live loads		
Residential	2.00	kN/m^2

Table 2 Design loads for the six-storey building

Type of load	Value	Unit
Structural permanent loads		
Slab self-weight	3.00	kN/m^2
Non-structural permanent loads		
Floor finish and screed	0.80	kN/m^2
Partitions (roof excluded)	1.20	kN/m^2
Live loads		
Residential	2.00	kN/m^2

Table 3 Material properties (see also Fig. 6)

Concrete	Reinforcing steel
$f_c = f_{pcu} = 37050$ kN/m^2	$f_y = 450000$ kN/m^2
epsc0=0.002	E_0=2.1 E+08 kN/m^2
epsU=0.01	b=0.01

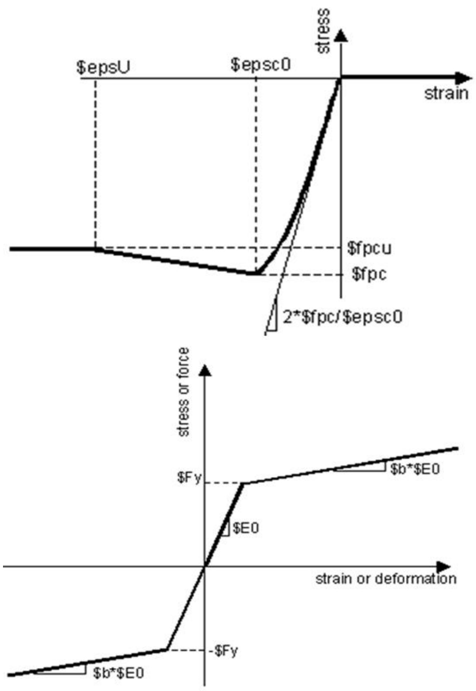

Fig. 6 OpenSees uniaxial materials: Concrete01 and Steel01

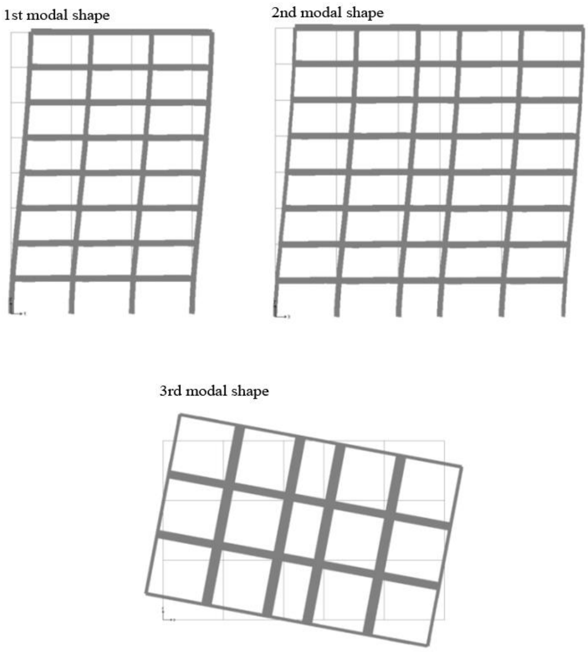

Fig. 7 Eight-storey building, 1st, 2nd and 3rd modal shapes

fundamental mode is mode 2, the mass participation ratio for the two buildings is equal to 0.54 and 0.81.

3.3 Engineering demand parameters

In order to investigate the effects of the variability of the direction of the ground motion on the structural demand, three Engineering Demand Parameters (EDPs) are considered:

Table 4 Eight and six-storey buildings: Dynamic properties after gravity loads application

	Eight-storey	Six-storey
N° Modal shape	Period (s)	Period (s)
1	T_1=2.47	T_1=1.34
2	T_2=1.81	T_2=1.24
3	T_3=1.69	T_3=1.02

- the Inter-storey Drift Ratio (IDR), with its distribution along the height of the building,
- the Maximum Inter-storey Drift Ratio (MIDR) over all stories,
- and the maximum roof horizontal displacement (U).

The IDR is defined as the maximum value over time (i.e., record duration) of the inter-storey drift ratio calculated as follows

$$IDR_i = \frac{\sqrt{\Delta x_i^{\,2} + \Delta y_i^{\,2}}}{h_i} \tag{1}$$

where:

- Δx_i and Δy_i are the drifts along the X and Y axes, respectively, between the centre of mass of the i^{th} and the $(i-1)^{th}$ floor,
- h_i is the storey height.

The MIDR is simply the maximum IDR value along the height of the building.

4. Effects of the seismic incidence

This section presents the results of the structural analyses, and discusses the effects of the GM incidence angle on the response of the buildings. Figs. 8-9 show the IDR distribution produced by a single record (no.14) with different angles of incidence, obtained with the 3D frame models of the eight-storey and the six-storey buildings, respectively.

It may be noted that in the eight-storey building for this specific record the MIDR is higher in cases 3 and 4, which correspond to angles of incidence of 45° and 67.5°, respectively. However, for the other records considered, different angles were observed producing a higher MIDR value. This means that the critical angle strongly depends not only on the properties of the structure but also on the characteristics of the signal. In the six-storey building excited by record no.14, the MIDR is higher in cases 7 and 8, i.e. when the incidence angle is equal to 135° and 157.5°. This variability in the critical angle with the exciting record considered is clearly shown in Fig.10. The figure reports the MIDR value obtained for the eight-storey building using records no.16 and no.18 and varying angles of incidence: in the first case (i.e., record no.16), the critical angle is 45° while in the second case (record no.18), it is 180°.

Figs. 11 and 12 show the MIDR obtained for the eight- and six-storey buildings, respectively, by varying the incidence angle. For the sake of clarity, only 50 records are

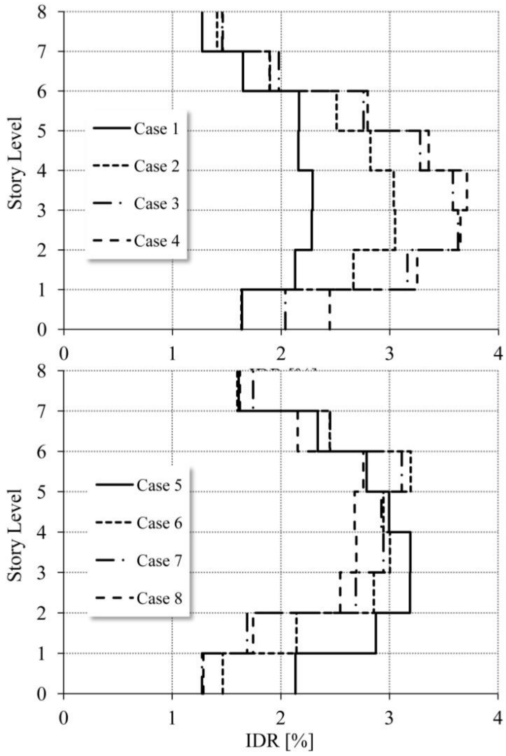

Fig. 8 Eight-storey building: IDR distribution along the height, for different GM incidence angles

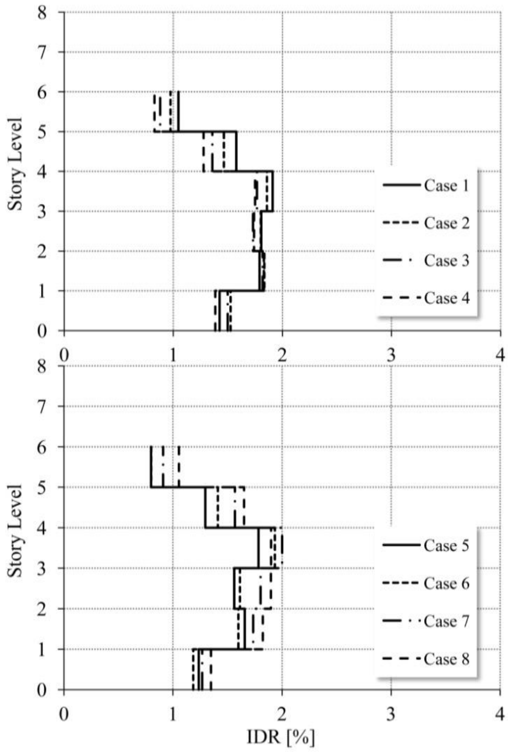

Fig. 9 Six-storey building: IDR distribution along the height, for different GM incidence angles

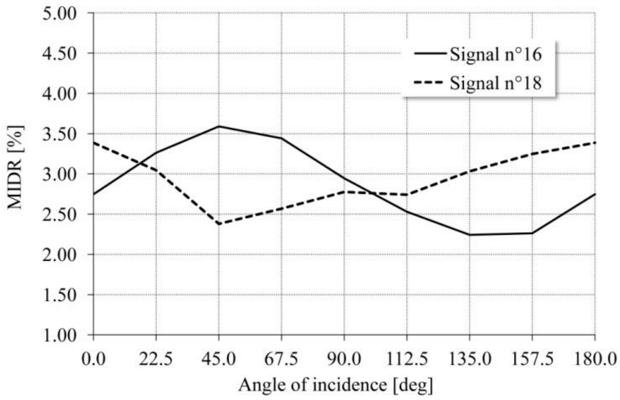

Fig. 10 Eight-storey building: MIDR values obtained for the records no.16 and 18 by varying the incidence angle

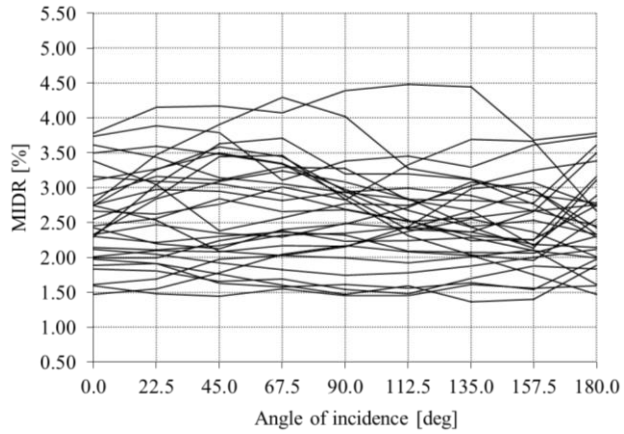

Fig. 11 Eight-storey building: MIDR values obtained with different records by varying the incidence angle

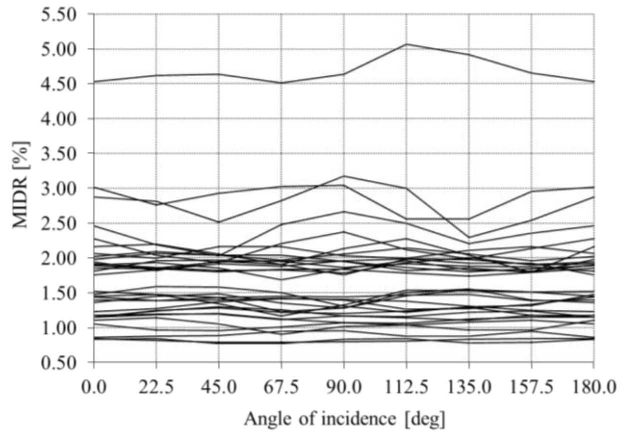

Fig. 12 Six-storey building: MIDR values obtained with different records by varying the incidence angle

reported in the figures. However, they are representative, in terms of variability of MIDR, of the whole database.

The significant difference between the two cases reveals that the critical angle of incidence is clearly a function of the dynamic properties of the building. This means that identifying the critical angle requires the analysis of the specific structure, that is, a high computational effort.

And besides, the critical angle strongly depends on the properties of the exciting record. This is clearly shown also in Figs. 13-14, which show the same results as Figs. 11-12, but, for the sake of clarity, for few records only, by using a different type of plot.

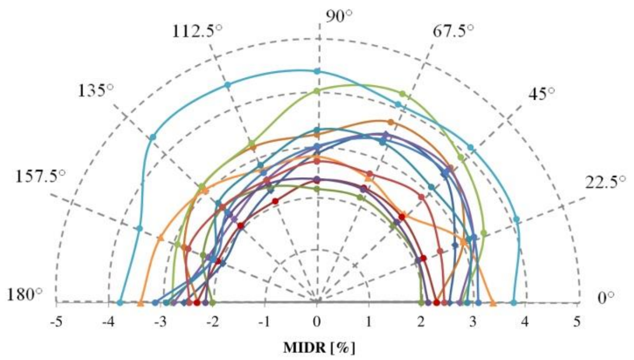

Fig. 13 Eight-storey building: MIDR values obtained for selected records by varying the incidence angle

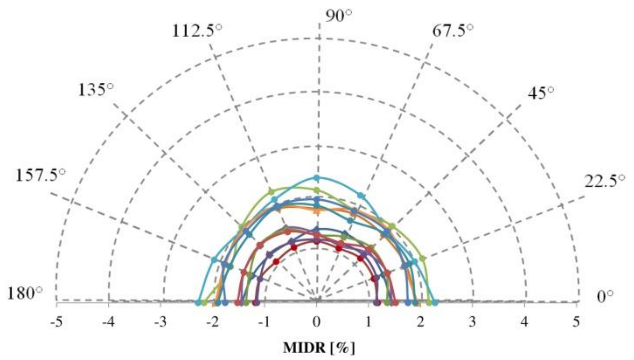

Fig. 14 Six-storey building: MIDR values obtained for selected records by varying the incidence angle

5. Evaluation of the proposed procedure

5.1 Equivalent 2DOF models of the structure

This section describes the calibration of the simplified model. Actually, two alternatives for the equivalent 2DOF model are considered: a linear model (L) and a non-linear (elasto-perfectly-plastic) model (NL). The properties of the two models are determined using the approach proposed by Eurocode 8 (2004), which is based on the calculation of capacity curves along the two in-plan directions of a building. For each direction, the capacity curve, represented by a base shear force-roof displacement relationship, is obtained through pushover analysis. Lateral forces proportional to the 1st and 2nd mode of vibration of the building are used in the analysis along the Y and X direction, respectively. For each push-over curve an idealised elasto-perfectly-plastic force-displacement relationship is derived as follows. The yield force F_y^*, which represents also the strength of the idealised system, is determined as the maximum base shear force at the formation of the plastic mechanism. The initial stiffness of the idealised system is determined in such a way that the areas under the actual and the idealised force-deformation curves are equal. The displacement limit considered to calculate the areas is that related to the maximum shear. Based on these assumptions, the yield displacement of the idealised single degree of freedom (SDOF) system d_y^* is given by

Table 5 Eight-storey building: Parameters characterizing the properties of the simplified models along the X axis

Parameter	Value	Unit
Yield force F_y^*	8515	kN
Yield displacement d_y^*	0.308	m
Equivalent stiffness $k^*= F_y^*/ d_y^*$	27626	kN m^{-1}
Equivalent mass m^*	3083	kN m^{-1}s^2
Equivalent period T^*	2.10	s

Table 6 Eight-storey building: Parameters characterizing the properties of the simplified models along the Y axis

Parameter	Value	Unit
Yield force F_y^*	6296	kN
Yield displacement d_y^*	0.434	m
Equivalent stiffness $k^*= F_y^*/ d_y^*$	14445	kN m^{-1}
Equivalent mass m^*	3246	kN m^{-1}s^2
Equivalent period T^*	2.98	s

Table 7 Six-storey building: Parameters characterizing the properties of the simplified models along the X axis

Parameter	Value	Unit
Yield force F_y^*	5957	kN
Yield displacement d_y^*	0.238	m
Equivalent stiffness $k^*= F_y^*/ d_y^*$	25060	kN m^{-1}
Equivalent mass m^*	1541	kN m^{-1}s^2
Equivalent period T^*	1.56	s

Table 8 Six-storey building: Parameters characterizing the properties of the simplified models along the Y axis

Parameter	Value	Unit
Yield force F_y^*	5660	kN
Yield displacement d_y^*	0.310	m
Equivalent stiffness $k^*= F_y^*/ d_y^*$	18237	kN m^{-1}
Equivalent mass m^*	1474	kN m^{-1}s^2
Equivalent period T^*	1.79	s

$$d_y^* = 2\left(d_m^* - \frac{E_m^*}{F_y^*}\right) \tag{2}$$

where d_m^* and E_m^* are the displacement and the deformation energy values at the maximum shear, respectively. Once F_y^* and d_y^* are determined, the period T^* of the equivalent SDOF system is calculated as follows

$$T^* = 2\pi\sqrt{\frac{m^* d_y^*}{F_y^*}} \tag{3}$$

where

$$m^* = \sum_{i=1}^{n} m_i \phi_i \tag{4}$$

Table 9 EDPs used in the comparison between the results obtained with the 3D and the simplified models

EDP	Description
$U^{3D}(\vartheta)$	Roof displacement U a obtained with the 3D model by varying incidence angle ϑ
$MIDR^{3D}(\vartheta)$	Maximum Inter-storey Drift Ratio MIDR obtained with the 3D model by varying incidence angle ϑ
$\vartheta^{3D}{}_{cr}$	Critical incidence angle that provides, for each record considered, the maximum value of U^{3D} or $MIDR^{3D}$, i.e. $U^{3D}(\vartheta^{3D}{}_{cr})$ and $MIDR^{3D}(\vartheta^{3D}{}_{cr})$, respectively
U^L U^{NL}	Displacements obtained with the simplified 2DOF linear (L) and non-linear (NL) models, respectively
$\vartheta^L{}_{cr}$ $\vartheta^{NL}{}_{cr}$	Critical angles of incidence that provide, for each record considered, the maximum value of U^L (i.e., $U^L(\vartheta^L{}_{cr})$) and U^{NL} (i.e., $U^{NL}(\vartheta^{NL}{}_{cr})$), respectively

m_i and ϕ_i are the mass and the normalized displacement of the i[th] floor, respectively. Parameter T^* is used to set the properties of the equivalent linear model, and F_y^* and d_y^* those of the non-linear one. The values obtained of these parameters in the case of the eight- and six-storey building are given in Tables 5-6 and Tables 7-8, respectively.

5.2 Critical incidence angle

In order to evaluate the predictive accuracy of the simplified models, different comparisons are carried out. By using the eight angles of incidence and the set of 124 signals, 992 non-linear time-history analyses are performed for each building model. For each record, the critical angle $\vartheta^{3D}{}_{cr}$ is defined as the one that provides the maximum structural responses $U^{3D}(\vartheta^{3D}{}_{cr})$ or $MIDR^{3D}(\vartheta^{3D}{}_{cr})$. The values of $\vartheta^{3D}{}_{cr}$, $U^{3D}(\vartheta^{3D}{}_{cr})$ and $MIDR^{3D}(\vartheta^{3D}{}_{cr})$ are obtained from the non-linear analyses of the 3D buildings. Similarly, $\vartheta^L{}_{cr}$ and $\vartheta^{NL}{}_{cr}$ are defined as the critical angles that provide the maximum displacement values $U^L(\vartheta^L{}_{cr})$ and $U^{NL}(\vartheta^{NL}{}_{cr})$ in the simplified linear and non-linear model, respectively.

To evaluate the relationship between the different parameters considered, linear regressions are performed between the EDPs given in Table 9. In particular, the following pairs of EDPs are analysed in order to assess the predictive ability of the simplified models:

- $U^L(\vartheta^L{}_{cr})$ vs. $U^{3D}(\vartheta^{3D}{}_{cr})$ (see Figs. 15(a) and 16(a) for the eight- and six-storey buildings, respectively), to evaluate the ability of the linear 2DOF model to predict the maximum displacement;
- $U^{NL}(\vartheta^{NL}{}_{cr})$ vs. $U^{3D}(\vartheta^{3D}{}_{cr})$ (see Figs. 15(b) and 16(b) for the eight- and six-storey buildings, respectively), to evaluate the ability of the non-linear 2DOF model to predict the maximum displacement;
- $MIDR^{3D}(\vartheta^{3D}{}_{cr})$ vs. $MIDR^{3D}(\vartheta^L{}_{cr})$ (see Figs. 17(a) and 18(a) for the eight- and six-storey models, respectively), to compare the MIDR values calculated using the 3D model when the critical angle is obtained from the analyses of the 3D model ($\vartheta^{3D}{}_{cr}$) or from those of the linear 2DOF model ($\vartheta^L{}_{cr}$);
- $MIDR^{3D}(\vartheta^{3D}{}_{cr})$ vs. $MIDR^{3D}(\vartheta^{NL}{}_{cr})$ (see Figs. 17(b) and 18(b) for the eight- and six-storey models, respectively), to compare the MIDR values calculated using the 3D model when the critical angle is obtained from the analyses of the 3D model ($\vartheta^{3D}{}_{cr}$) or from those of the non-linear 2DOF model ($\vartheta^{NL}{}_{cr}$);
- $U^{3D}(\vartheta^{3D}{}_{cr})$ vs. $U^{3D}(\vartheta^L{}_{cr})$ (see Figs. 19(a) and 20(a) for the eight- and six-storey models, respectively), to make a comparison similar to $MIDR^{3D}(\vartheta^{3D}{}_{cr})$ vs. $MIDR^{3D}(\vartheta^L{}_{cr})$ but in terms of displacements;
- $U^{3D}(\vartheta^{3D}{}_{cr})$ vs. $U^{3D}(\vartheta^{NL}{}_{cr})$ (Figs. 19(b) and 20(b) for the eight- and six-storey models, respectively), to make a comparison similar to $MIDR^{3D}(\vartheta^{3D}{}_{cr})$ vs. $MIDR^{3D}(\vartheta^{NL}{}_{cr})$ but in terms of displacements.

In brief, in each figure, the graph denoted with (a) compares the maximum response obtained from the 3D non-linear model with the response obtained using its equivalent linear 2DOF counterpart. Analogously, the graph denoted with (b) compares the former with its equivalent non-linear 2DOF counterpart.

Values μ and σ given in Figs. 15-20 are the mean and the standard deviation of ratio α between the two parameters considered. For instance, in Fig. 15(a) α is

$$\alpha = \frac{U^L(\vartheta^L{}_{cr})}{U^{3D}(\vartheta^{3D}{}_{cr})} \tag{5}$$

Note that, in some cases, large inter-storey drift ratio and roof displacement values are obtained. In particular, for some exciting records, the inter-storey drift ratio is larger than 0.04 (conventional value corresponding to collapse according to FEMA 356), and the roof drift ratio is larger than 0.03. Even if such large values might correspond to collapse states, they were not excluded from the regression analyses. The debate on the definition of collapse criteria for buildings, in fact, is still open (Terrenzi *et al.* 2018) and falls outside the scope of this study. However, in Figs. 15-20 conventional collapse limits are shown, i.e., 0.04 for the inter-storey drift ratio and to 0.03 for the roof drift ratio (leading to two different roof displacement values for the two buildings).

It is also interesting to note that the displacements U of the 2DOF models are in general larger than those obtained with the 3D models, especially in the case of the linear 2DOF ones (Figs. 15(a) and 16(a)). In the case of the non-linear 2DOF models (Figs. 15(b) and 16(b)), better predictions are obtained. This can be attributed to the fact that the structural response achieves the inelastic range for 80% of the records.

Figs. 17-20 can be used to evaluate the suitability of the critical incidence angles estimated from the simplified models. These figures show, in particular, the response obtained with the 3D model under the record oriented along the critical incidence angle determined using the 3D (fully 3D analysis) or the simplified model (proposed procedure). In each plot, the abscissa gives the response evaluated through the simplified model, whereas the ordinate gives the actual (exact) response derived from the 3D model. Figs. 17-18 show the response expressed in terms of maximum drift, $MIDR^{3D}$, and Figs. 19-20 in terms of top displacement, U^{3D}. It can be observed that there is broad agreement between the two results, with the mean, μ, between 0.89 and 0.94 and the dispersion, σ, the same as or smaller than 0.1. The best predictions are obtained for the

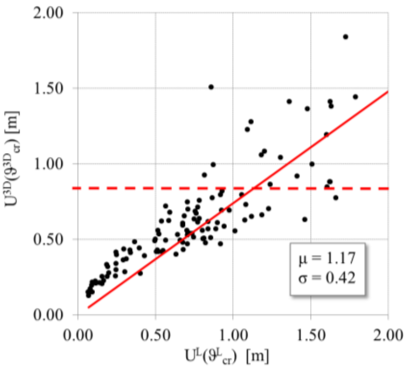

(a)

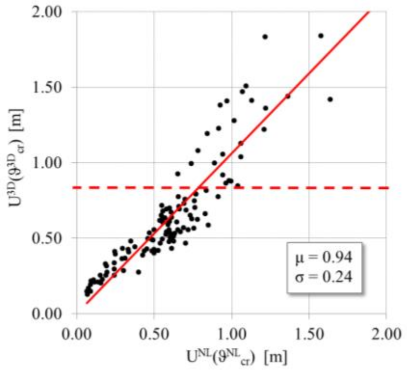

(b)

Fig. 15 Comparison of U in the eight-storey building obtained with the 3D and the 2DOF models: (a) linear 2DOF model, (b) non-linear 2DOF model

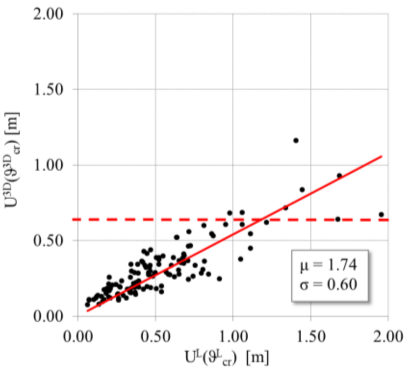

(a)

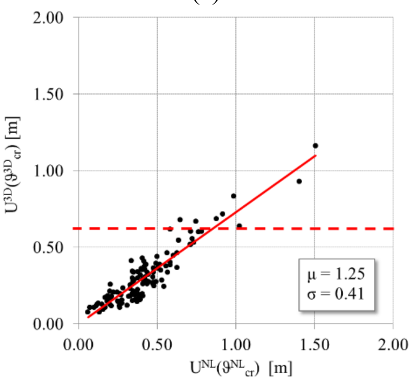

(b)

Fig. 16 Comparison of U in the six-storey building obtained with the 3D and the 2DOF models: (a) linear 2DOF model, (b) non-linear 2DOF model

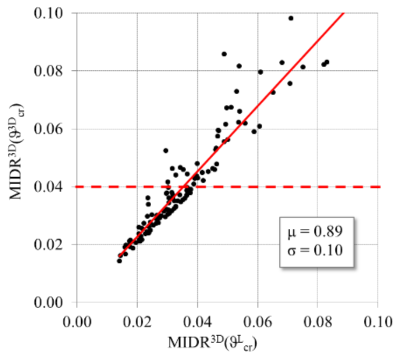

(a)

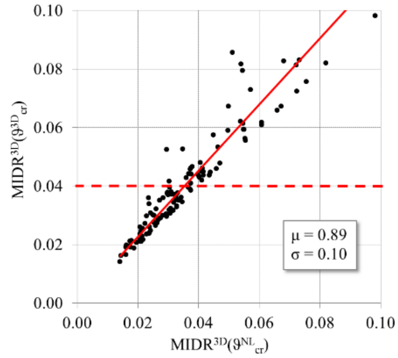

(b)

Fig. 17 Comparison of MIDR in the eight-storey building obtained with the 3D model by using ϑ^{3D}_{cr} and: (a) ϑ^{L}_{cr} (obtained with the linear 2DOF model), (b) ϑ^{NL}_{cr} (obtained with the non-linear 2DOF model)

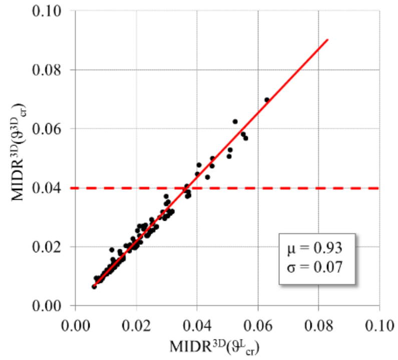

(a)

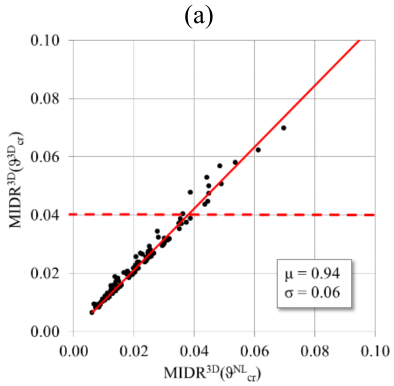

(b)

Fig. 18 Comparison of MIDR in the six-storey building obtained with the 3D model by using ϑ^{3D}_{cr} and: (a) ϑ^{L}_{cr} (obtained with the linear 2DOF model), (b) ϑ^{NL}_{cr} (obtained with the non-linear 2DOF model)

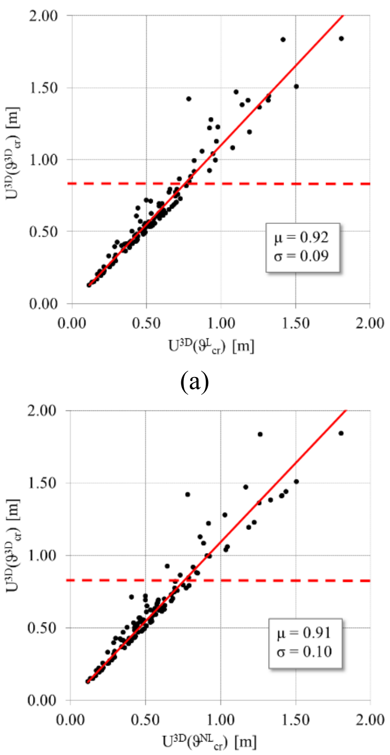

(a)

(b)

Fig. 19 Comparison of U in the eight-storey building obtained with the 3D model by using ϑ^{3D}_{cr} and: (a) ϑ^{L}_{cr} (obtained with the linear 2DOF model), (b) ϑ^{NL}_{cr} (obtained with the non-linear 2DOF model)

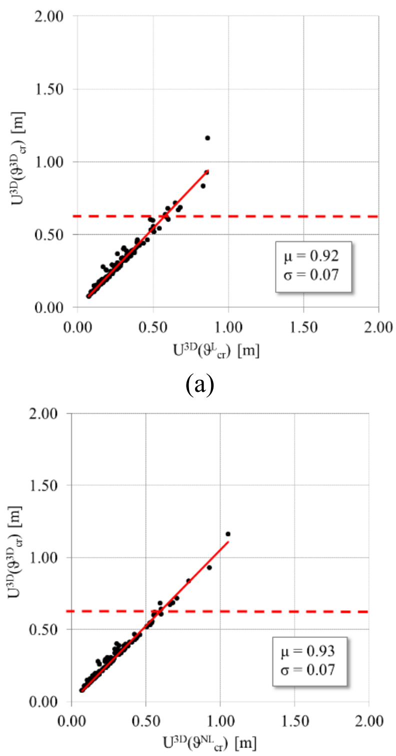

(a)

(b)

Fig. 20 Comparison of U in the six-storey building obtained with the 3D model by using ϑ^{3D}_{cr} and: (a) ϑ^{L}_{cr} (obtained with the linear 2DOF model), (b) ϑ^{NL}_{cr} (obtained with the non-linear 2DOF model)

six-storey frame, but also for the eight-story building the results are satisfactory, especially in the case of the U^{3D} prediction. It is important to note that if the EDP values beyond the collapse limits were excluded, the σ values would further reduce.

Summarising, although the 2DOF models do not always provide an accurate prediction of the EDPs, they provide an adequate estimate of the critical angle. Moreover, the use of the non-linear 2DOF model with respect to the linear 2DOF model does not produce a significant improvement in the prediction of the critical angle.

6. Conclusions

This work puts forward a procedure to predict the most critical incidence angle of the seismic load for buildings subjected to near-fault ground motions. Current seismic codes do not usually include detailed indications regarding the direction of application of the seismic load that produces the most critical effects, whereas this aspect is of particular relevance, especially in near-fault conditions for irregular as well as regular buildings. As a consequence, multiple analyses of the structure are required which consider different possible ground motion incidence angles. In this context, the procedure proposed aims at reducing the computational effort that derives from such analyses when a 3D model is used to estimate the response.

Buildings designed according to a former seismic code are analysed in this study. However, the proposed procedure can be adopted also for the analysis of new buildings, especially those whose structural characteristics along the two in-plan directions differ significantly from one another and for which, as a consequence, the determination of the critical incidence angle is of primary importance.

The procedure is based on the use of an equivalent 2DOF model to represent the building, thus reducing the computational effort required to estimate the critical angle. The steps of the procedure are summarised in Fig. 1. First, a 3D non-linear model of the building is created, and non-linear static pushover analyses are performed in the two principal in-plan directions. The capacity curves obtained are then used to derive the parameters of an equivalent 2DOF model. The 2DOF model is subjected to the selected ground motion by varying the incidence angle in order to evaluate the most critical incidence angle, ϑ_{cr}, which causes the maximum displacement U in the model. Finally, a non-linear time-history analysis of the 3D model with the selected ground motion applied along the angle ϑ_{cr} is performed to obtain the structural response associated with the most critical condition. If an ensemble of ground motions is necessary for the analysis of the structure, the procedure has to be repeated for each GM of the set.

The proposed procedure is validated by analysing two reinforced concrete buildings, eight- and six-storey tall, subjected to a set of 124 near-fault ground motions applied along 8 different incidence angles. The structures are designed according to the Italian DM96 code in order to represent existing buildings. Based on the results obtained for the two case studies analysed, the following conclusions can be drawn.

- The structural demand expressed in terms of inter-storey drift depends significantly on the incidence angle also for buildings regular in plan such as the ones considered.
- The incident angle that causes the highest structural response depends on the characteristics of both the ground motion and the structure, as shown in Fig. 13 and 14, where the results obtained for a selection of records is shown for the two buildings.
- Figs. 17-20 highlight that the use of the critical angle calculated by means of the equivalent 2DOF model instead of the one calculated with the 3D model is adequate. Indeed, the differences obtained in terms of roof displacements and inter-storey drifts are small.
- Finally, the use of a non-linear 2DOF model in lieu of a linear 2DOF model does not lead to significant improvements in the prediction of the critical incidence angle. Thus, the use of the simpler linear model is recommended for building types similar to those analysed in the present study.

Acknowledgments

Partial funding from the Italian Civil Protection (project DPC-ReLUIS 2014-2016) and the Ministry of Education, University and Research (MIUR) are gratefully acknowledged. The opinions, findings, and conclusions or recommendations are of the authors, and do not necessarily reflect those of the sponsors.

References

ASCE/SEI 7-10 (2010), *Minimum Design Loads for Buildings and Other Structures*, American Society of Civil Engineers, Structural Engineering Institute, Reston, Virginia, U.S.A.

Athanatopoulou, A.M. (2005), "Critical orientation of three correlated seismic components", *Eng. Struct.*, **27**(2), 301-312.

Baker, J.W. (2007), "Quantitative classification of near-fault ground motions using wavelet analysis", *Bullet. Seismol. Soc. Am.*, **97**(5), 1486-1501.

Cantagallo, C., Camata, G. and Spacone, E. (2012), "The effect of the earthquake incidence angle on seismic demand of reinforced concrete structures", *Proceedings of the 15th World Conference on Earthquake Engineering*, Lisboa, Portugal, September.

Cantagallo, C., Camataa, G. and Spacone, E. (2015), "Influence of ground motion selection methods on seismic directionality effects", *Earthq. Struct.*, **8**(1), 185-204.

Cao, V.V. and Ronagh, H.R. (2014), "Correlation between parameters of pulse-type motions and damage of low-rise RC frames", *Earthq. Struct.*, **7**(3), 365-384.

Chopra, A.K. and Chintanapakdee, C. (2001), "Comparing response of SDF systems to near-fault and far-fault earthquake motions in the context of spectral regions", *Earthq. Eng. Struct. Dyn.*, **30**, 1769-1789.

Decanini, L.D., Liberatore, L. and Mollaioli, F. (2012), "Damage potential of the 2009 L'Aquila, Italy, earthquake", *J. Earthq. Tsunami*, **6**(3), 1-32.

DM 96 (1996), *Norme Tecniche per le Costruzioni in Zone Sismiche*, Decreto Ministeriale 16 Gennaio 1996, Ministero dei Lavori Pubblici, Rome, Italy.

Emami, A.R. and Halabian, A.M. (2005), "Spatial distribution of ductility demand and damage index in 3D RC frame structures considering directionality effects", *Struct. Des. Tall Spec. Build.*, **24**(16), 941-996.

Eurocode 8 (2004), *Design of Structures for Earthquake Resistance. Part 1: General Rules, Seismic Actions and rules for Buildings*, European Committee for Standardization; Brussels, Belgium.

FEMA 356 (2000), *Pre-standard and Commentary for the Seismic Rehabilitation of Buildings*, Federal Emergency Management Agency, Washington, U.S.A.

Fontara, I.K.M., Kostinakis, K.G. and Athanatopoulou, A.M. (2012), "Some issues related to the inelastic response of buildings under bi-directional excitation", *Proceedings of the 15th World Conference on Earthquake Engineering*, Lisboa, Portugal, September.

Haselton, C.B., Liel, A.B., Deierlein, G.G., Dean, B.S. and Chou, J.H. (2011), "Seismic collapse safety of reinforced concrete buildings: I. Assessment of ductile moment frames", *J. Struct. Eng.*, **137**(4), 481-491.

Hosseini, M. and Salemi, A. (2008), "Studying the effect of earthquake excitation on the internal forces of steel building's elements by using non-linear time history analyses", *Proceedings of the 14th World Conference on Earthquake Engineering*, Beijing, China, October.

ICBO (2010), *California Building Code, International Conference for Building Officials*, Whittier, California, U.S.A.

Kalkan, E. and Kunnath, S.K. (2006), "Effects of fling step and forward directivity on seismic response of buildings", *Earthq. Spectr.*, **22**(2), 367-390.

Kalkan, E. and Kwong, N.S. (2014), "Pros and cons of rotating ground motion records to fault-normal/parallel directions for response history analysis of buildings", *J. Struct. Eng.*, **140**(3), 04013062.

Liel, A.B., Haselton, C.B. and Deierlein, G.G. (2011), "Seismic collapse safety of reinforced concrete buildings: II. Comparative assessment of non-ductile and ductile moment frames", *J. Struct. Eng.*, **137**(4), 492-502.

Mazza, F., Mazza, M. and Vulcano, A. (2017), "Non-linear response of r.c. framed buildings retrofitted by different base-isolation systems under horizontal and vertical components of near-fault earthquakes", *Earthq. Struct.*, **12**(1), 135-144.

Mavroeidis, G.P. and Papageorgiou, A.S. (2003), "A mathematical representation of near-fault ground motions", *Bullet. Seismol. Soc. Am.*, **93**(3), 1099-1131.

McKenna, F. (1997), "Object-oriented finite element programming: frameworks for analysis, algorithms, and parallel computing", Ph.D. Dissertation, Department of Civil and Environmental Engineering, University of California, Berkeley, U.S.A.

Mollaioli, F., Bruno, S., Decanini, L.D. and Panza, G.F. (2006), "Characterization of the dynamical response of structures to damaging pulse-type near-fault ground motions", *Meccan.*, **41**, 23-46.

Mollaioli, F., Liberatore, L. and Lucchini, A. (2014), "Displacement damping modification factors for pulse-like and ordinary records", *Eng. Struct.*, **78**, 17-27.

Moustafa, A. and Takewaki, I. (2010), "Characterization and modeling of near-fault pulse-like strong ground motion via damage-based critical excitation method", *Struct. Eng. Mech.*, **6**, 755-778.

NEHRP (2004), *Recommended Provisions for Seismic Regulations for New Buildings and Other Structures*, National Earthquake Hazards Reduction Program, Building Seismic Safety Council of the National Institute of Building Sciences, Washington, U.S.A.

Reyes, J.C. and Kalkan, E. (2015), "Significance of rotating ground motions on behavior of symmetric- and asymmetric-plan structures: Part I. single-story structures", *Earthq. Spectr.*, **31**(3), 1591-1612.

Rigato, A.B. and Medina, R.A. (2007), "Influence of angle of incidence on seismic demands for inelastic single-storey structures subjected to bi-directional ground motions", *Eng. Struct.*, **29**, 2593-2601.

Somerville, P.G., Smith, N.F., Graves, R.W. and Abrahamson, N.A. (1997), "Modification of empirical strong ground motion attenuation relations to include the amplitude and duration effects of rupture directivity", *Seismol. Res. Lett.*, **68**(1), 199-222.

Tabatabaei, R. and Saffari H. (2011), "Influence of near-fault ground motions characteristics on elastic seismic response of asymmetric buildings", *Struct. Eng. Mech.*, **40**(4), 489-500.

Terrenzi, M., Spacone, E. and Camata, G. (2018), "Collapse limit state definition for seismic assessment of code-conforming RC buildings", *Int. J. Adv. Struct. Eng.*

Tsourekas, A.G., Athanatopoulou, A.M. and Avramidis, I.E. (2009), "Effects of seismic incident angle on response of structures under bi-directional recorded and artificial ground motion", *Proceedings of the 2nd International Conference on Computational Methods in Structural Dynamics and Earthquake Engineering, Thematic Conference*, Island of Rhodes, Greece, June.

CC

Appendix

Table 10 Main properties of the ground motions used in the analyses

Num	Earthquake Name	Year	Station Name	M	EpiD (km)	HypD (km)	ClstD (km)	NEHRP Based on Vs30	PGA (g)	PGV (cm/sec)	PGD (cm)
001	Managua, Nicaragua-01	1972	Managua, ESSO	6.2	5.7	7.6	4.1	D	0.39	25.35	6.4
002	Gazli, USSR	1976	Karakyr	6.8	12.8	22.3	5.5	C	0.64	61.50	20.8
003	Coyote Lake	1979	Gilroy Array #6	5.7	4.4	9.1	3.1	C	0.40	37.09	6.5
004	Imperial Valley-06	1979	Brawley Airport	6.5	43.2	44.3	10.4	D	0.18	37.68	18.1
005	Imperial Valley-06	1979	EC County Center FF	6.5	29.1	30.7	7.3	D	0.21	49.02	28.0
006	Imperial Valley-06	1979	EC Meloland Overpass FF	6.5	19.4	21.8	0.1	D	0.30	70.28	28.1
007	Imperial Valley-06	1979	El Centro Array #10	6.5	26.3	28.1	6.2	D	0.20	46.42	23.8
008	Imperial Valley-06	1979	El Centro Array #11	6.5	29.4	31.1	12.5	D	0.37	36.72	17.6
009	Imperial Valley-06	1979	El Centro Array #3	6.5	28.7	30.3	12.9	E	0.26	42.06	20.1
010	Imperial Valley-06	1979	El Centro Array #4	6.5	27.1	28.9	7.1	D	0.40	69.89	39.3
011	Imperial Valley-06	1979	El Centro Array #5	6.5	27.8	29.5	4.0	D	0.44	72.15	46.2
012	Imperial Valley-06	1979	El Centro Array #6	6.5	27.5	29.2	1.4	D	0.41	83.89	48.1
013	Imperial Valley-06	1979	El Centro Array #7	6.5	27.6	29.4	0.6	D	0.41	78.29	37.7
014	Imperial Valley-06	1979	El Centro Array #8	6.5	28.1	29.8	3.9	D	0.52	52.90	30.5
015	Imperial Valley-06	1979	El Centro Differential Array	6.5	27.2	29.0	5.1	D	0.42	56.21	30.6
016	Imperial Valley-06	1979	Holtville Post Office	6.5	19.8	22.2	7.7	D	0.23	47.47	29.0
017	Irpinia, Italy-01	1980	Sturno	6.9	30.4	31.8	10.8	B	0.29	43.74	21.5
018	Westmorland	1981	Westmorland Fire Sta	5.9	7.0	7.4	6.5	D	0.41	41.41	10.9
019	Westmorland	1981	Parachute Test Site	5.9	20.5	20.6	16.7	D	0.21	35.27	18.9
020	Coalinga-05	1983	Oil City	5.8	4.6	8.7		C	0.68	33.34	3.9
021	Coalinga-05	1983	Transmitter Hill	5.8	6.0	9.5		C	0.88	38.53	5.5
022	Coalinga-07	1983	Coalinga-14th & Elm (Old CHP)	5.2	9.6	12.7		D	0.58	28.91	3.4
023	Morgan Hill	1984	Anderson Dam (Downstream)	6.2	16.7	18.7	3.3	C	0.34	28.53	5.4
024	Morgan Hill	1984	Gilroy Array #6	6.2	36.3	37.3	9.9	C	0.27	23.52	4.1
025	N. Palm Springs	1986	Desert Hot Springs	6.1	10.4	15.1	6.8	D	0.34	26.10	4.9
026	N. Palm Springs	1986	North Palm Springs	6.1	10.6	15.3	4.0	D	0.61	50.05	8.1
027	San Salvador	1986	Geotech Investig Center	5.8	7.9	13.5	6.3	C	0.63	54.29	12.4
028	San Salvador	1986	National Geografical Inst	5.8	9.5	14.5	7.0	D	0.49	62.83	12.8
029	Whittier Narrows-01	1987	Downey - Co Maint Bldg	6.0	16.0	21.7	20.8	D	0.18	19.28	2.6
030	Whittier Narrows-01	1987	LB - Orange Ave	6.0	20.7	25.3	24.5	D	0.21	20.18	3.0
031	Whittier Narrows-01	1987	Santa Fe Springs - E.Joslin	6.0	11.7	18.7	18.5	D	0.43	28.29	3.3
032	Superstition Hills-02	1987	El Centro Imp. Co. Cent	6.5	35.8	36.9	18.2	D	0.29	45.16	18.1
033	Superstition Hills-02	1987	Parachute Test Site	6.5	16.0	18.4	1.0	D	0.44	71.85	34.0
034	Loma Prieta	1989	Gilroy Array #2	6.9	29.8	34.5	11.1	D	0.35	34.94	8.9
035	Loma Prieta	1989	Gilroy Array #3	6.9	31.4	35.9	12.8	D	0.46	43.11	11.8
036	Loma Prieta	1989	LGPC	6.9	18.5	25.4	3.9	C	0.78	77.15	42.7
037	Loma Prieta	1989	Saratoga - Aloha Ave	6.9	27.2	32.4	8.5	C	0.39	46.13	20.7
038	Loma Prieta	1989	Saratoga - W Valley Coll.	6.9	27.1	32.2	9.3	C	0.31	57.09	25.7
039	Erzican, Turkey	1992	Erzincan	6.7	9.0	12.7	4.4	D	0.50	68.77	24.1
040	Cape Mendocino	1992	Cape Mendocino	7.0	10.4	14.1	7.0	C	1.35	90.38	27.8

M = Magnitude, EpiD = Epicentral Distance, HypD = Hypocentral Distance, ClstD = Closest Distance, NEHRP = National Earthquake Hazards Reduction Program soil type, PGA = Peak Ground Acceleration, PGV = Peak Ground Velocity, PGD = Peak Ground Displacement

Table 10 Main properties of the ground motions used in the analyses (Continued)

Num	Earthquake Name	Year	Station Name	M	EpiD (km)	HypD (km)	ClstD (km)	NEHRP Based on Vs30	PGA (g)	PGV (cm/sec)	PGD (cm)
041	Cape Mendocino	1992	Petrolia	7.0	4.5	10.5	8.2	C	0.59	69.59	25.7
042	Landers	1992	Lucerne	7.3	44.0	44.6	2.2	C	0.74	97.16	164.3
043	Landers	1992	Yermo Fire Station	7.3	86.0	86.3	23.6	D	0.21	37.74	30.7
044	Northridge-01	1994	Jensen Filter Plant	6.7	13.0	21.8	5.4	C	0.75	74.25	30.9
045	Northridge-01	1994	Jensen Filter Plant Generator	6.7	13.0	21.8	5.4	C	0.75	74.57	32.0
046	Northridge-01	1994	LA - Sepulveda VA Hospital	6.7	8.5	19.5	8.4	C	0.80	74.13	16.3
047	Northridge-01	1994	LA Dam	6.7	11.8	21.1	5.9	C	0.46	56.35	19.0
048	Northridge-01	1994	Newhall - Fire Sta	6.7	20.3	26.8	5.9	D	0.70	81.83	26.1
049	Northridge-01	1994	Newhall - W Pico Canyon Rd.	6.7	21.6	27.8	5.5	D	0.39	78.15	39.3
050	Northridge-01	1994	Pacoima Dam (downstr)	6.7	20.4	26.9	7.0	A	0.41	35.19	4.7
051	Northridge-01	1994	Rinaldi Receiving Sta	6.7	10.9	20.6	6.5	D	0.66	109.32	30.3
052	Northridge-01	1994	Sylmar - Converter Sta	6.7	13.1	21.9	5.4	D	0.71	108.13	49.7
053	Northridge-01	1994	Sylmar - Converter Sta East	6.7	13.6	22.2	5.2	C	0.65	90.59	31.9
054	Northridge-01	1994	Sylmar - Olive View Med FF	6.7	16.8	24.2	5.3	C	0.68	94.35	22.9
055	Kobe, Japan	1995	KJMA	6.9	18.3	25.6	1.0	D	0.71	77.83	18.9
056	Kobe, Japan	1995	Kobe University	6.9	25.4	31.1	0.9	B	0.78	83.57	19.7
057	Kobe, Japan	1995	Port Island (0 m)	6.9	19.3	26.3	3.3	D	0.32	73.09	35.3
058	Kobe, Japan	1995	Takarazuka	6.9	38.6	42.6	0.3	D	0.69	75.78	22.2
059	Kobe, Japan	1995	Takatori	6.9	13.1	22.2	1.5	D	0.64	116.29	32.3
060	Northwest China-03	1997	Jiashi	6.1	19.1	27.7		D	0.29	28.88	4.6
061	Kocaeli, Turkey	1999	Arcelik	7.5	53.7	56.0	13.5	C	0.17	28.45	25.8
062	Kocaeli, Turkey	1999	Duzce	7.5	98.2	99.5	15.4	D	0.33	55.32	29.6
063	Kocaeli, Turkey	1999	Gebze	7.5	47.0	49.7	10.9	B	0.18	38.22	31.6
064	Kocaeli, Turkey	1999	Yarimca	7.5	19.3	25.1	4.8	D	0.31	60.51	54.7
065	Chi-Chi, Taiwan	1999	CHY006	7.6	40.5	41.3	9.8	C	0.36	52.04	20.4
066	Chi-Chi, Taiwan	1999	CHY024	7.6	24.1	25.4	9.6	C	0.23	50.15	34.3
067	Chi-Chi, Taiwan	1999	CHY028	7.6	32.7	33.6	3.1	C	0.79	71.98	18.2
068	Chi-Chi, Taiwan	1999	CHY035	7.6	43.9	44.6	12.7	C	0.26	39.00	13.6
069	Chi-Chi, Taiwan	1999	CHY101	7.6	32.0	33.0	10.0	D	0.39	90.70	57.7
070	Chi-Chi, Taiwan	1999	TAP003	7.6	151.7	151.9	102.4	D	0.11	31.40	18.5
071	Chi-Chi, Taiwan	1999	TCU029	7.6	79.2	79.6	28.1	C	0.18	48.47	42.5
072	Chi-Chi, Taiwan	1999	TCU031	7.6	80.1	80.5	30.2	C	0.13	49.32	42.1
073	Chi-Chi, Taiwan	1999	TCU034	7.6	87.9	88.2	35.7	C	0.20	37.85	32.9
074	Chi-Chi, Taiwan	1999	TCU036	7.6	67.8	68.3	19.8	D	0.13	54.03	55.8
075	Chi-Chi, Taiwan	1999	TCU038	7.6	73.1	73.6	25.4	D	0.15	45.45	52.0
076	Chi-Chi, Taiwan	1999	TCU040	7.6	69.0	69.5	22.1	C	0.13	49.64	52.7
077	Chi-Chi, Taiwan	1999	TCU042	7.6	78.4	78.8	26.3	D	0.21	43.00	36.7
078	Chi-Chi, Taiwan	1999	TCU046	7.6	68.9	69.4	16.7	C	0.12	34.78	30.0
079	Chi-Chi, Taiwan	1999	TCU049	7.6	38.9	39.7	3.8	C	0.27	53.87	58.1
080	Chi-Chi, Taiwan	1999	TCU050	7.6	41.5	42.2	9.5	D	0.14	39.56	53.4
081	Chi-Chi, Taiwan	1999	TCU052	7.6	39.6	40.4	0.7	C	0.35	131.95	183.2

Table 10 Main properties of the ground motions used in the analyses (Continued)

Num	Earthquake Name	Year	Station Name	M	EpiD (km)	HypD (km)	ClstD (km)	NEHRP Based on Vs30	PGA (g)	PGV (cm/sec)	PGD (cm)
082	Chi-Chi, Taiwan	1999	TCU053	7.6	41.2	42.0	6.0	C	0.18	44.67	52.4
083	Chi-Chi, Taiwan	1999	TCU054	7.6	37.6	38.5	5.3	C	0.17	48.69	53.5
084	Chi-Chi, Taiwan	1999	TCU056	7.6	39.7	40.5	10.5	D	0.14	39.82	49.1
085	Chi-Chi, Taiwan	1999	TCU057	7.6	41.8	42.5	11.8	C	0.11	38.05	53.4
086	Chi-Chi, Taiwan	1999	TCU059	7.6	53.4	54.0	17.1	D	0.16	58.54	58.5
087	Chi-Chi, Taiwan	1999	TCU060	7.6	45.4	46.1	8.5	D	0.15	38.05	50.6
088	Chi-Chi, Taiwan	1999	TCU063	7.6	35.5	36.4	9.8	C	0.15	57.01	55.5
089	Chi-Chi, Taiwan	1999	TCU064	7.6	59.1	59.7	16.6	D	0.12	50.98	47.4
090	Chi-Chi, Taiwan	1999	TCU065	7.6	26.7	27.9	0.6	D	0.66	101.64	77.9
091	Chi-Chi, Taiwan	1999	TCU068	7.6	47.9	48.5	0.3	C	0.53	204.65	336.2
092	Chi-Chi, Taiwan	1999	TCU075	7.6	20.7	22.2	0.9	C	0.29	58.77	58.6
093	Chi-Chi, Taiwan	1999	TCU076	7.6	16.0	17.9	2.8	C	0.36	58.73	30.7
094	Chi-Chi, Taiwan	1999	TCU082	7.6	36.2	37.1	5.2	C	0.22	52.69	60.4
095	Chi-Chi, Taiwan	1999	TCU087	7.6	55.6	56.2	7.0	C	0.12	44.83	47.2
096	Chi-Chi, Taiwan	1999	TCU098	7.6	99.7	100.1	47.7	C	0.11	35.82	35.6
097	Chi-Chi, Taiwan	1999	TCU101	7.6	45.1	45.8	2.1	D	0.22	57.12	52.9
098	Chi-Chi, Taiwan	1999	TCU102	7.6	45.6	46.3	1.5	C	0.25	87.49	75.8
099	Chi-Chi, Taiwan	1999	TCU103	7.6	52.4	53.0	6.1	C	0.16	44.47	53.1
100	Chi-Chi, Taiwan	1999	TCU104	7.6	49.3	49.9	12.9	C	0.11	43.71	50.8
101	Chi-Chi, Taiwan	1999	TCU106	7.6	37.7	38.5	15.0	C	0.16	44.33	37.2
102	Chi-Chi, Taiwan	1999	TCU111	7.6	44.8	45.5	22.1	D	0.11	43.58	39.8
103	Chi-Chi, Taiwan	1999	TCU116	7.6	24.4	25.7	12.4	C	0.17	47.18	37.6
104	Chi-Chi, Taiwan	1999	TCU122	7.6	21.8	23.2	9.4	C	0.24	38.82	35.5
105	Chi-Chi, Taiwan	1999	TCU128	7.6	63.3	63.8	13.2	C	0.15	66.12	73.0
106	Chi-Chi, Taiwan	1999	TCU136	7.6	48.8	49.4	8.3	C	0.17	48.42	55.6
107	Chi-Chi, Taiwan	1999	WGK	7.6	32.0	33.0	10.0	D	0.39	70.27	53.4
108	Chi-Chi, Taiwan-03	1999	CHY024	6.2	25.5	26.7	19.7	C	0.13	23.54	14.5
109	Chi-Chi, Taiwan-03	1999	CHY080	6.2	29.5	30.5	22.4	C	0.33	47.46	8.7
110	Chi-Chi, Taiwan-03	1999	TCU076	6.2	20.8	22.2	14.7	C	0.33	39.60	6.3
111	Duzce, Turkey	1999	Bolu	7.1	41.3	43.6	12.0	D	0.77	59.68	17.7
112	Duzce, Turkey	1999	Duzce	7.1	1.6	14.1	6.6	D	0.43	70.77	47.3
113	Yountville	2000	Napa Fire Station #3	5.0	9.9	14.2	11.5	D	0.51	36.16	3.3
114	Bam, Iran	2003	BAM	6.6	12.59	13.94	4.8	C	0.74	88.28	27.2
115	Parkfield	2004	Cholame 1E	6.0	11.44	14.02	3	D	0.39	39.72	8.5
116	Parkfield	2004	Cholame 2W	6.0	11.54	14.10	3.01	E	0.48	48.31	9.9
117	Parkfield	2004	Cholame 3W	6.0	12.17	14.62	3.63	D	0.41	34.26	6.2
118	Parkfield	2004	Cholame 4W	6.0	12.32	14.74	4.23	C	0.56	30.10	4.4
119	Parkfield	2004	Fault Zone 1 (COW)	6.0	8.40	11.67	2.51	E	0.64	67.33	10.8
120	Parkfield	2004	Eades	6.0	9.95	12.83	2.85	C	0.36	26.33	6.3
121	Parkfield	2004	Fault Zone 12 (PRK)	6.0	10.99	13.66	2.65	D	0.29	42.44	10.6
122	Parkfield	2004	Stone Corral (SC1)	6.0	7.17	10.82	3.79	D	0.72	38.37	4.7
123	Parkfield	2004	Cholame 3E	6.0	11.87	14.37	5.55	C	0.65	25.42	2.8
124	Parkfield	2004	Fault Zone 14	6.0	8.68	11.87	8.81	D	1.04	68.77	13.5